IPTC-19228-MS

Comprehensive Seismic Data Conditioning of the Bioclastic Limestone in the Middle East

Tengfei Lin, Xueling Wang, and Junchang Dong, Department of Middle East E&P, RIPED

Abstract

The bioclastic limestone reservoirs of Cretaceous period occupy an important position in the petroleum industry of Middle East. It is the carbonate heterogeneity that is challenging the accuracy of the reservoir prediction, which brings forward higher requirements for the seismic data quality. Besides, some seismic data are processed more than 10 years ago, the signal to noise ratio (SNR) is relative low due to the random noise and coherent noise like acquisition footprint anomalies. The acquisition footprint artifacts caused by acquisition and processing seriously suppress the true stratigraphic features, which can result in pitfalls in seismic interpretation, seismic attribute analysis as well as seismic inversion. While the pre-stack seismic data is usually unavailable, which means that the noise can hardly be subtracted by conventional pre-stack seismic processing workflows, such as statics, high-resolution velocity analysis and ground roll attenuation. Consequently, a comprehensive post-stack seismic data conditioning workflow is necessary to solve the above problems.

In order to improve the post-stack seismic data quality, a comprehensive data conditioning workflow are applied for noise suppression. Firstly, structural-oriented filtering is utilized to attenuate random noise and partial acquisition footprint artifacts. Then 2D waveform transform of seismic amplitude and filtered seismic attribute in x-y domain are calculated, to separate acquisition footprint anomalies (large wave number in kx-ky domain) from true structural signal (small wave number in kx-ky domain) by interactive analysis. The application of Laplace-Gaussian (LoG) filter deserves an obvious improvement in acquisition footprint suppression workflow. The comprehensive noise attenuation workflow in this paper can effectively remove both periodic and non-periodic noise to obtain higher signal to noise ratio (SNR) for post-stack seismic volume. In this way, the stratigraphic features (tidal-channel, reef-beach complex) can be more clearly depicted and some artifacts caused by noise will disappear in seismic attribute calculation, seismic inversion and reservoir prediction.

Introduction

The dip estimation method was firstly introduced based on the estimation of dip with the most coherent event (Gulunay et al., 1993). Luo et al. (1996) and Barnes (1996) created a method to estimate vector dip based on 3D extension of the analytic trace attributes. Finn (1986) realized the true 3D dip estimation, and then Marfurt et al. (1998a) extended to semblance-based scan according to Finn's idea. The seismic noise usually distributes along structural events, which means that the dip components can help to establish an accurate 3D structural filter to realize the structure-oriented filtering (Davogustto and Marfurt, 2011). In this way, the application of structure-oriented filtering can remove both random noise and partial coherent noise.

Acquisition footprint responses indicate the imprint of acquisition geometry caused in seismic acquisition and processing procedures. The acquisition footprint anomalies can result in interpretation artifacts (Marfurt and Alves, 2014; Cahoj et al., 2016), which greatly influence the 3D seismic interpretation and following seismic attributes analysis, especially for the structural attributes (dip components, coherence and curvature et al.) and reservoir prediction (Marfurt et al., 1998b). Hill et al. (1999) proved that acquisition footprint anomalies could be caused by inaccurate velocity analysis and NMO correction. By theoretical forward modeling, Cahoj et al. (2016) summarized the possible origins of acquisition footprint occurrence: residual ground roll, inaccurate velocity analysis, and far-offset migration stretch. The sources of this phenomenon determine that acquisition footprint will vanish from shallow to deep position gradually.

Ideally, the major problem in 3D seismic interpretation triggered by acquisition footprint artifacts can be eliminated through careful attenuation, such as trace balance statics, noise reduction and velocity analysis in seismic processing procedures (Hill et at., 1999; Gulunay, 2000). But the pre-stack seismic processing is unreachable for the seismic interpreter, and the geometry parameters (source and receiver coordinates) are not included in the post-stack seismic volume.

The amplitude anomalies caused by acquisition footprint responses can be detected in time or horizon slice of the shallow zone. Although acquisition footprint artifacts may not prevent a skilled interpreter to pick an accurate horizon, it is hard to realize auto-tracking. Besides, the patch-like amplitude anomalies always suppress the seismic responses caused by true geological features. For example, the reef-beach complex is the primary sweet spot in the bioclastic reservoir of Middle East, which usually is characterized as continuous positive seismic amplitude. While the existence of acquisition footprint artifacts will come up to a fragmentized sections, making it hard to separate from true structural signal.

Seismic attribute analysis is one of the effective interpretation-aided tools for structural and depositional feature delineation. Structural seismic attributes (dip components, coherence and curvature et al.) can depict the structural boundaries, such as faults, channel edges and high-fractured zones. Amplitude and energy seismic attributes can effectively indict the reservoir distribution as well as seismic facies characterization. While the existence of acquisition footprint anomlies can not only cause structural artifacts to confuse real geological features, but also cause "fake" seismic responses. Seismic attributes are more sensitive to acquisition footprint artifacts compared to the seismic amplitude volume, which means that they can enhance influence of the acquisition footprint artifacts. On the other hand, seismic attributes can be used to extract acquisition footprint anomalies

Because the distribution of acquisition footprint responses are controlled by source and receiver positions with periodic distribution, which usually is smaller compared to the true geological structures. It is the difference in wavenumber between acquisition footprint anomalies and the geological responses that provides theoretical foundaiton for acquisition footprint anomalies suppression in 2D waveform domain (Drummond et al., 2000; Falconer and Marfurt, 2006). Alali et al. (2016) applied 2D continuous wavelet transform (CWT) to suppress acquisition footprint responeses of post-stack seismic amplitude volume. Laplace-Gaussian (LoG) filter is a powerful tool for edge detection. The application of Laplace-Gaussian (LoG) filter in 2D waveform domain can further improve acquisition footprint responses (Lin et al., 2016).

In this paper, we proposed an attribute-assisted structure-oriented filtering workflow and an attribute-assisted footprint suppression workflow to comprehensively realize the seismic data conditioning of the bioclastic limestone reservoir in the Middle East.

Theories and Definitions

Kuwahara Filter

Kuwahara filter was first introduced by Kuwahara et al (1976) as an edge-preserved smoothing filter in medical imaging, and then standard deviation was come into use by Luo et al (2002). Marfurt (2006) extended Kuwahara filter to three dimensions, and computed coherence along structural direction.

In Kuwahara filter, the radius r_{Kuw} is set to create a 2D window. The analysis point will be put in the window center and several adjacent points will be chosen based on the distance between the analysis point and nearby points. Providing that inline spacing and crossline spacing are d_m and d_n, respectively:

$$M_{Kuw} = \mathrm{NINT}(r_{Kuw}, d_m), \quad (1)$$

$$N_{Kuw} = \mathrm{NINT}(r_{Kuw}, d_n), \quad (2)$$

where $2M_{Kuw} + 1$, $2N_{Kuw} + 1$, are the largest window size in inline and crossline direction, respectively. The adjacent points within the 2D window will be included for calculation. For instance, if $r_{Kuw} = 50$ m, and $d_m = d_n = 25$ m, then M_{Kuw} and N_{Kuw} will be 2, which means that a 5 by 5 2D window will be created (Figure 1).

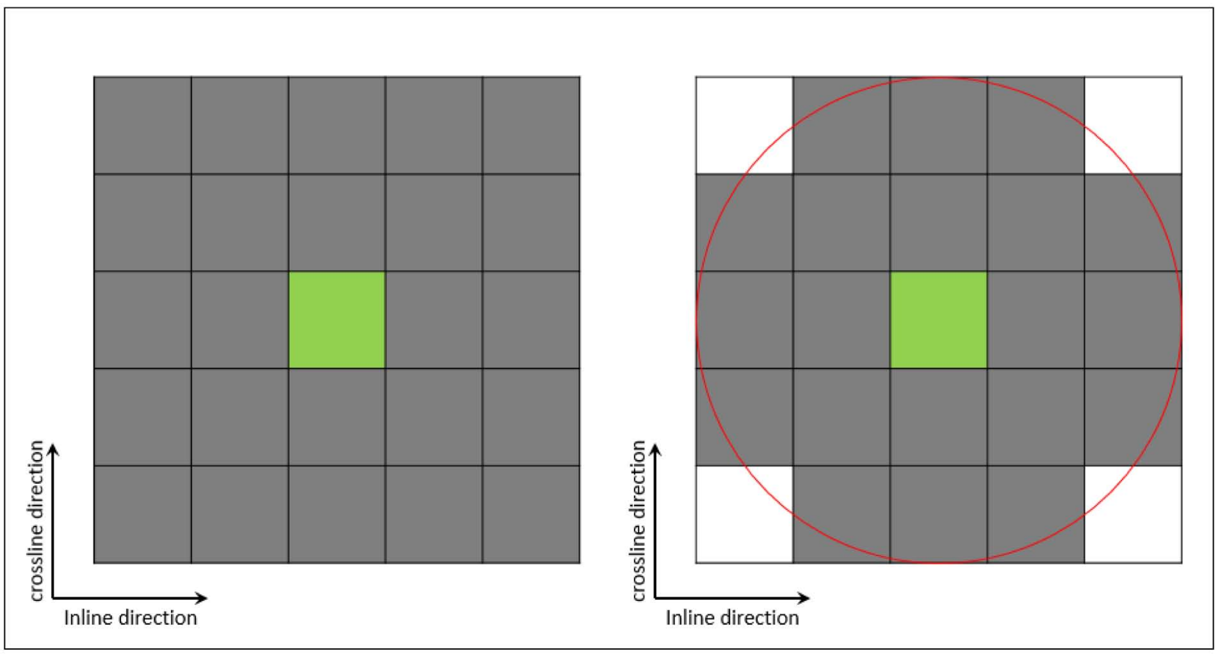

Figure 1—The diagram of 2D analysis (a) rectangular and (b) circle window.

Green bin in Figure 1 indicates the analysis point, and the surrounding grey bins indicate the adjacent points. 24 adjacent points will be selected if a rectangular window is preferred (Figure 1a), and 20 adjacent points be confirmed if a circle window is selected (Figure 1b).

The sub-window size of the Kuwahara filter is $2M_{Kuw} - 1$ in inline direction, and $2N_{Kuw} - 1$ in crossline direction. 9 different sub-windows are depicted in Figure 2, coherence is calculated in each sub-window and choose the one with the highest coherence value, to replace the analysis point with calculated mean value (Figure 2).

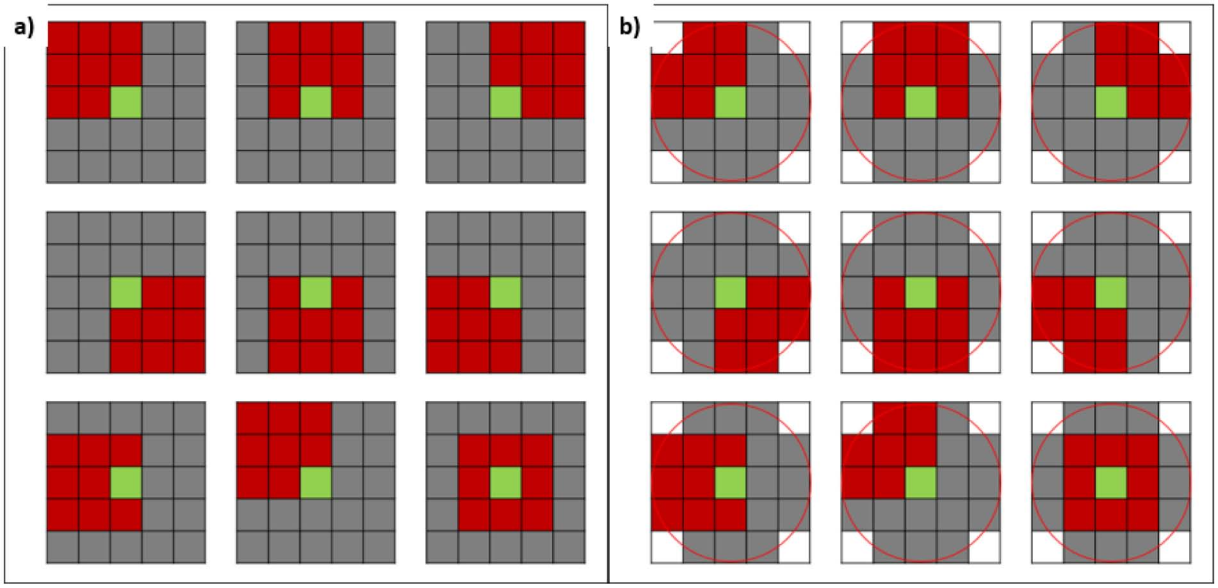

Figure 2—The diagram of 2D Kuwahara filter with (a) rectangular and (b) circle window.

The coherence attribute is widely used in fault detection, fluvial edge identification, which are characterized as low coherence value and should be preserved in the filter. While the existence of random noise and coherent noise also cause relative low coherence. The histogram of coherence attribute (Figure 3) indicates that most of the coherence values are distributed in large value (coherent zone indicated by black arrow). The filter will be prevented to keep the stratigraphic boundaries ($w_{SOF} = 0$) for small coherence value ($s < s_{low}$), be applied to smooth the signal ($w_{SOF} = 1$) for large coherence value ($s > s_{high}$), and be the combination of the mean value, u_{mean} and the original value, u_{orig} in the analysis point (Equation 3) for the rest ($s_{high} > s > s_{low}$):

$$w_{SOF} = (s - s_{low})/(s_{high} - s_{low}), \tag{3}$$

$$u_{SOF} = w_{SOF} \cdot u_{mean} + (1 - w_{SOF}) \cdot u_{orig}, \tag{4}$$

where w_{SOF} is defined as smooth weight, s_{high} and s_{low} are two threshold values which separate the structural features to be preserved from the noise to be smoothed.

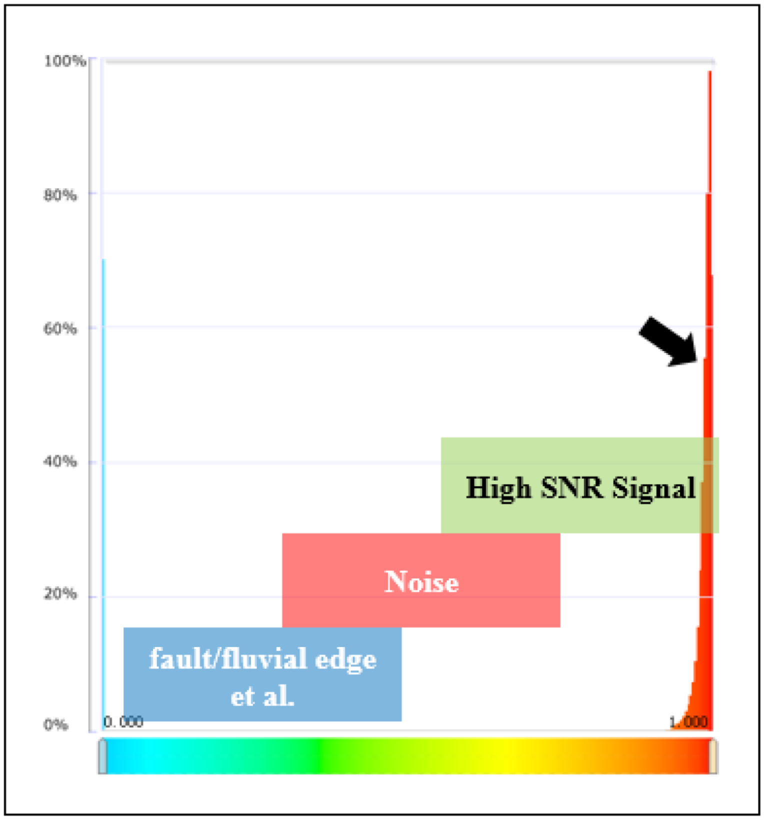

Figure 3—The histogram of coherence attribute.

Vertical Median Filter

Median filter is a non-linear filter, which usually is applied to suppress random noise, especially for speckle noise or salt-and-pepper noise. While the stratigraphic features and acquisition footprint anomalies indicate coherent seismic events, which can be preserved in the median filter. Figure 4a is a synthetic seismic trace with several spike noise and random noise. The spike anomalies and random noise (Figure 4c) can be separated from the original signal (Figure4a) to get the filtered one (Figure 4b). The application of vertical median filter to the seismic attribute sensitive to acquisition footprint anomalies can make the values of stratigraphic feature to be zero, and improve acquisition footprint artifacts.

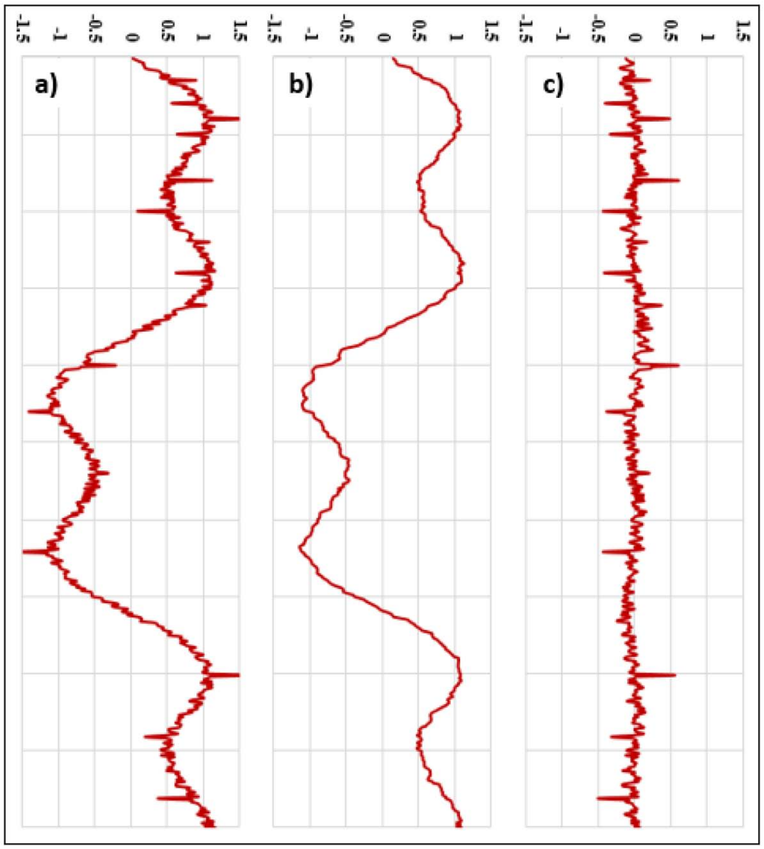

Figure 4—The median filter analysis (a. synthetic seismic trace with spike noise and random noise, b. the filtered result and c. the extracted noise) of a synthetic seismic trace.

2D Waveform Transform

Fourier Transform plays an important role in signal processing, including noise suppression, edge detection, signal separation and recovery et al. Fourier transform in time domain has been widely used in frequency analysis (Partyka et al., 1999; Bahorich et al., 2002; Liu and Marfurt, 2005&2007; Wang 2007&2010; Lin et. al., 2013&2018), 2D Fourier Transform of *f-k* domain is a powerful tool for noise suppression (Xu et al., 2005; Qin et al., 2012). For waveform transform, it can be designed to filter periodic and non-periodic noise (Buttkus, 2000). For 2D waveform transform, $U(k_x, k_y)$ in k_x-k_y domain can be expressed as below:

$$U(k_x,k_y)=\sum_{x=0}^{M_{2D}-1}\sum_{y=0}^{N_{2D}-1}u(x,y)e^{-j2\pi\left(\frac{x}{M_{2D}}k_x+\frac{y}{N_{2D}}k_y\right)}, \tag{5}$$

where x, y are inline and crossline number in spatial domain, respectively. M_{2D}, N_{2D} are wavenumber period in inline and crossline direction, respectively. k_x, k_y are wavenumber of inline and crossline direction, respectively. And $u(x, y)$ is the seismic signal in spatical domain.

$$U(k_x,k_y)=\left|U(k_x,k_y)\right|e^{-j\varphi(k_x,k_y)}, \tag{6}$$

where $|U(k_x, k_y)|$ is amplitude spectrum, and $\varphi(k_x, k_y)$ is phase spectrum of $U(k_x, k_y)$.

Considering the basic property of Fourier Transform, we can conclude that 2D waveform transform has both periodicity (Equation 7) and conjugate symmetry (Equation 8):

$$U(k_x,k_y)=U(k_x\pm m\cdot M_{2D},k_y\pm n\cdot N_{2D}) \qquad m=0,1,2,\cdots;\quad n=0,1,2,\cdots, \tag{7}$$

$$U(k_x,k_y)=U(\pm k_x,\pm k_y). \tag{8}$$

The large scale stratigraphic features mainly focus on the low-wavenumber zone, which is indicated by the red zone of 2D waveform transform in Figure 5. While acquisition footprint artifacts mainly follow the source-receiver positions, the source spacing and receiver spacing are smaller size compared to stratigraphic features, which indicate that acquisition footprint responses in k_x-k_y domain are characterized as relative large wavenumber (green zone in Figure 5), and being far away from the center of the amplitude spectrum in 2D waveform Transform. Besides, the responses will show up symmetrically (Equation 8) due to the conjugate symmetry.

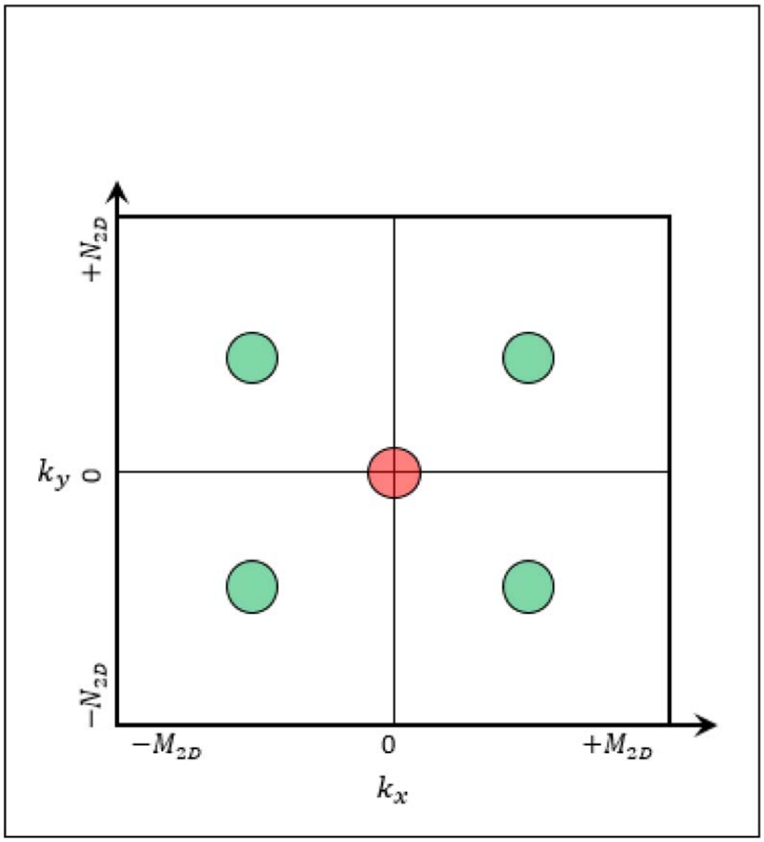

Figure 5—The diagram of amplitude spectrum in k_x-k_y domain.

Laplace-Gaussian (LoG) Filter

The Laplace operator is the divergence of the gradient. On one hand, it can improve the signal edges' responses. On the other hand, it can be easily affected by noise:

$$\Delta u(x,y) = \nabla \cdot \nabla u(x,y), \tag{9}$$

$$\Delta u(x,y) = \frac{\partial^2 u(x,y)}{\partial x^2} + \frac{\partial^2 u(x,y)}{\partial y^2}. \tag{10}$$

The Gaussian filter in spatial domain (Equation 11) can be expressed as Equation 12 in k_x-k_y domain:

$$log_\sigma(x,y) = \frac{1}{\sqrt{2\pi\sigma^2}} \cdot e^{\left(-\frac{x^2 + y^2}{2\sigma^2}\right)}, \tag{11}$$

$$LoG_\sigma(k_x,k_y) = \frac{1}{\pi\sigma^2} \cdot \left(1 - \frac{k_x^2+k_y^2}{2\sigma^2}\right) \cdot e^{\left(-\frac{k_x^2+k_y^2}{2\sigma^2}\right)}. \tag{12}$$

The Gaussian filter is universally applied to suppress the noise and improve signal to noise ratio (SNR), especially for the noise that follow normal distribution, because it can enhance the edge detection while suppressing the noise. The Laplace-Gaussian filter (Marr and Hildreth, 1980), the combination of Laplace operator and Gaussian filter, was introduced to solve the defects of Laplace operator.

For a special time slice, we can convert seismic attribute $u_{attr}(x, y)$ (sensitive to acquisition footprint anomalies) from spatial domain to $U_{attr}(k_x, k_y)$ of 2D wavenumber domain. Then we apply Laplace-Gaussian (LoG) filter, $LoG_\sigma(k_x, k_y)$, to better image acquisition footprint anomalies.

Weighted Factor

Since seismic amplitude follows Gaussian distribution, the relevant energy mainly focus in the center zone of k_x-k_y domain. The difference between the values of the centered zone (small wavenumber) and the surrounding area (large wavenumber zone) is huge. It is the acquisition footprint responses that distribute in large wavenumber zone, forming periodic high energy responses in the amplitude spectrum of k_x-k_y domain. In order to better identify acquisition footprint responses of k_x-k_y domain, a weighted factor w_k is designed to enhance the responses after the application of Laplace-Gaussian (LoG) filter:

$$w_k\left(k_x, k_y\right) = e^{\left(\frac{|k|}{|k|_{max}}\right)}, \tag{13}$$

where

$$|k| = \left(k_x^2 + k_y^2\right)^{1/2}, \tag{14}$$

$$|k|_{max} = max\left[\left(k_x^2 + k_y^2\right)^{1/2}\right]. \tag{15}$$

The ultimate result in k_x-k_y domain after Laplace-Gaussian filtering and factor weighting can be expressed as following:

$$U_{wgt}(k_x, k_y) = U_{attr}(k_x, k_y) \cdot LoG_\sigma\left(k_x, k_y\right) \cdot w_k\left(k_x, k_y\right). \tag{16}$$

Applications

The reservoirs of Cretaceous period in the Middle East develop massive bioclastic limestone with buried depth about 3,000 m, which belong to the carbonate platform sedimentary system. The seismic amplitude volume (Figure 6) acquired in the Middle East is suffering from random noise as well as acquisition footprint anomalies. Figures 6a and 6b indicate the time slice and corresponding seismic profile along AA'. The zooned in section (Figure 6c) of the red polygon shows V-shape artifacts, which seriously disturb the stratigraphic responses. Since some seismic attributes are sensitive to acquisition footprint anomalies, we can found that Figures 7a and 7b describe the dip magnitude slice and coherence slice of Figure 6a, respectively. The red dashed polygon encloses the patch-like anomalies due to acquisition footprint artifacts, which seriously suppress true structural information (black arrow). The application of comprehensive seismic data conditioning workflow to the seismic amplitude volume above acquired in the Middle East can effectively remove random noise and acquisition footprint anomalies after attribute-assisted structure-oriented filtering and attribute-assisted acquisition footprint suppression.

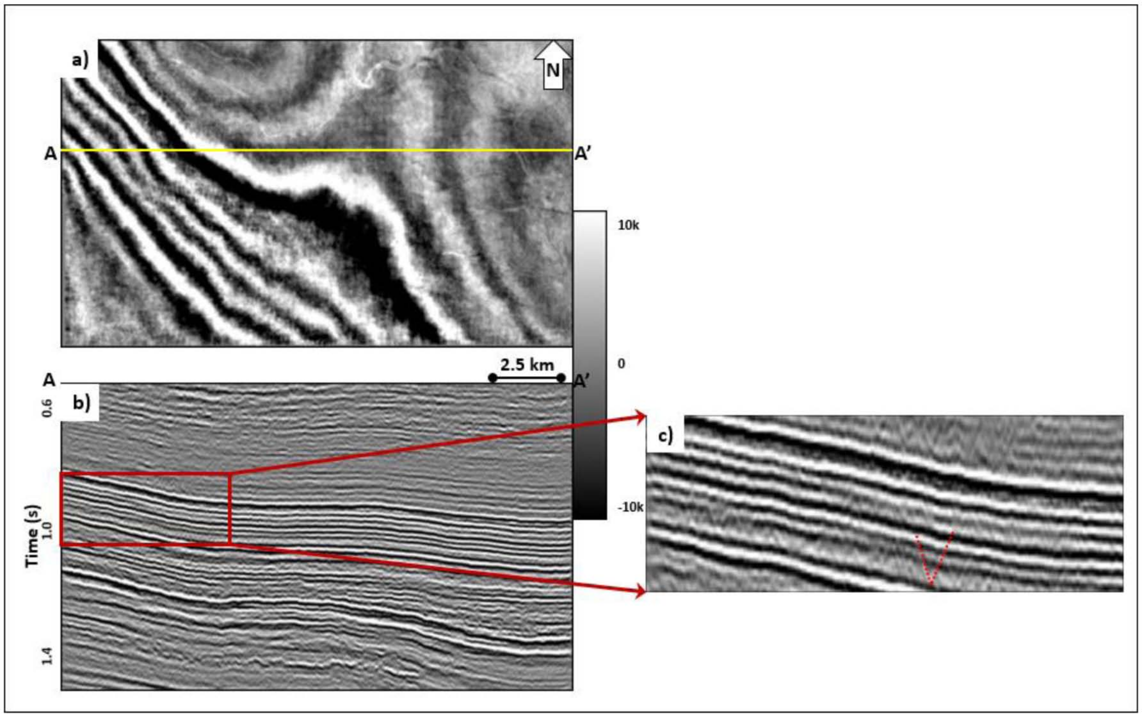

Figure 6—a) Time slice and b) corresponding seismic profile along AA', and c) zooned in section (Figure 6b) of the original seismic amplitude volume.

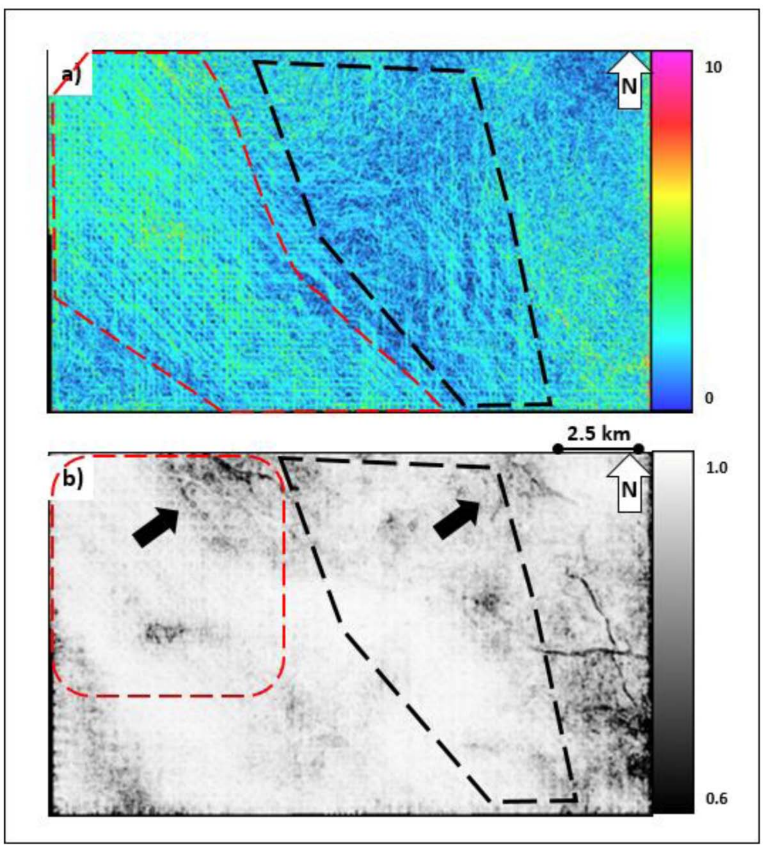

Figure 7—a) Dip magnitude slice and b) coherence slice of the original seismic amplitude volume.

Attribute-Assisted Structure-Oriented Filtering

Figure 8 indicates the workflow of attribute-assisted structure-oriented filtering. Coherence is a powerful tool for the fault and channel edge detection, which are characterized as low values in coherence. The filter will be neglected if *s* is smaller than the threshold value, to realize edge-preservation, and be applied if *s* is larger than the threshold value, to suppress noise and improve signal to noise ratio (SNR).

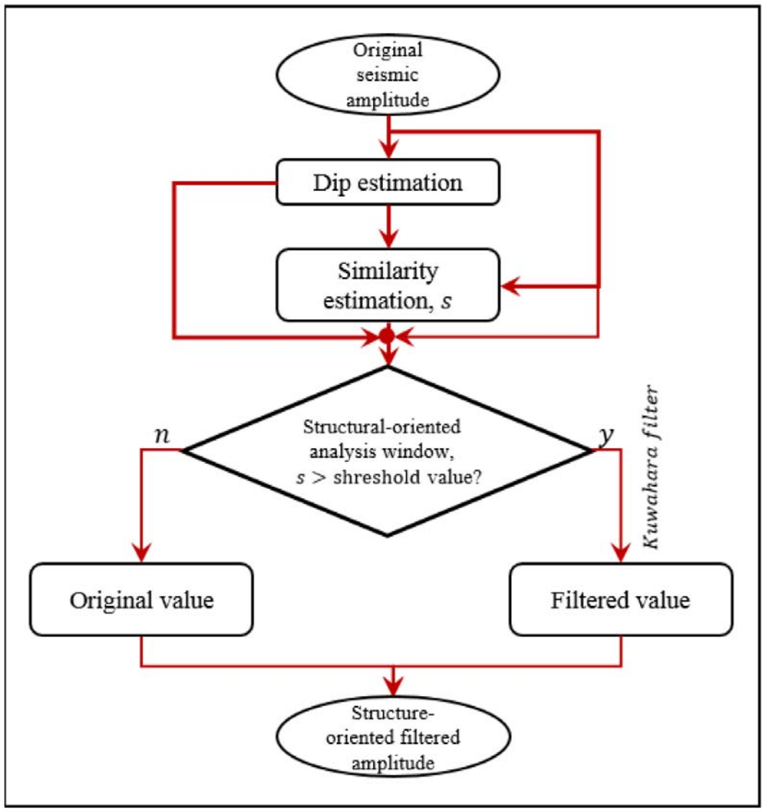

Figure 8—The workflow of attributed-assisted structure-oriented filtering.

Figure 9 gives us the time slice and corresponding seismic profile along AA' of the seismic amplitude volume after attribute-assisted structure-oriented filtering. The zooned in section (Figure 9c) of the red polygon shows the filtered results. The V-shape artifacts have been removed in Figure 9c compared to the one in Figure 6c. Figure 10 indicates the difference between the original seismic amplitude and the one after structure-oriented filtering.

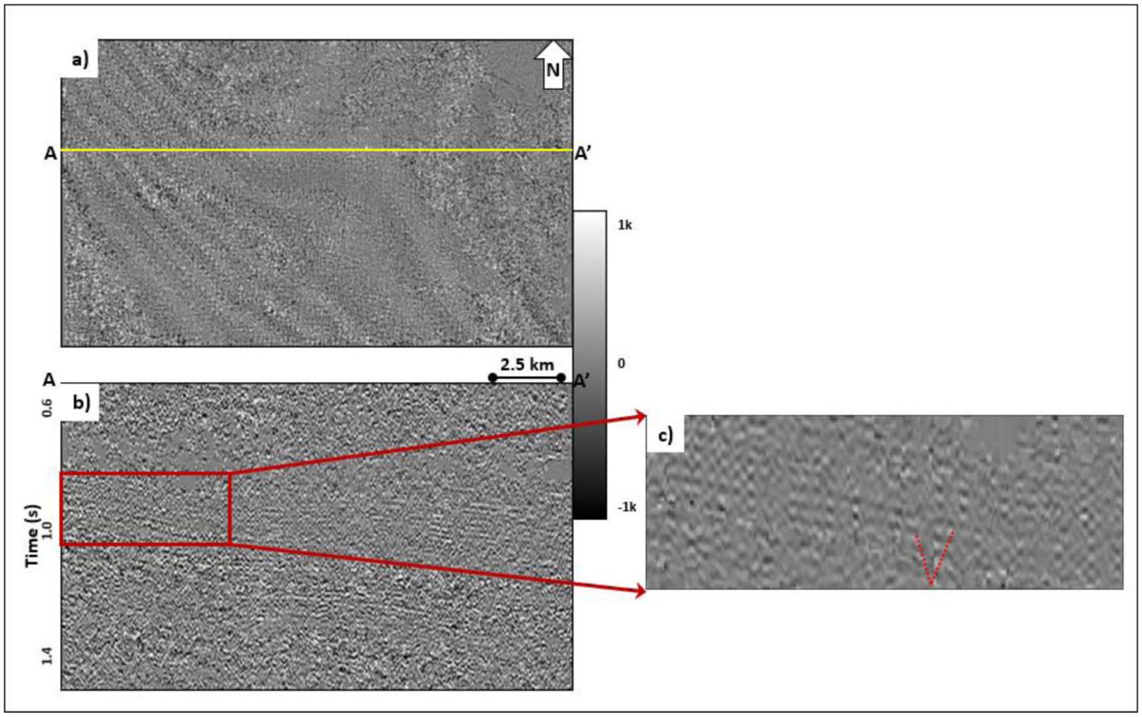

Figure 9—a) Time slice and b) corresponding seismic profile along AA', and c) zooned in section (Figure 11b) of the difference between original seismic amplitude volume and the one after structure-oriented filtering.

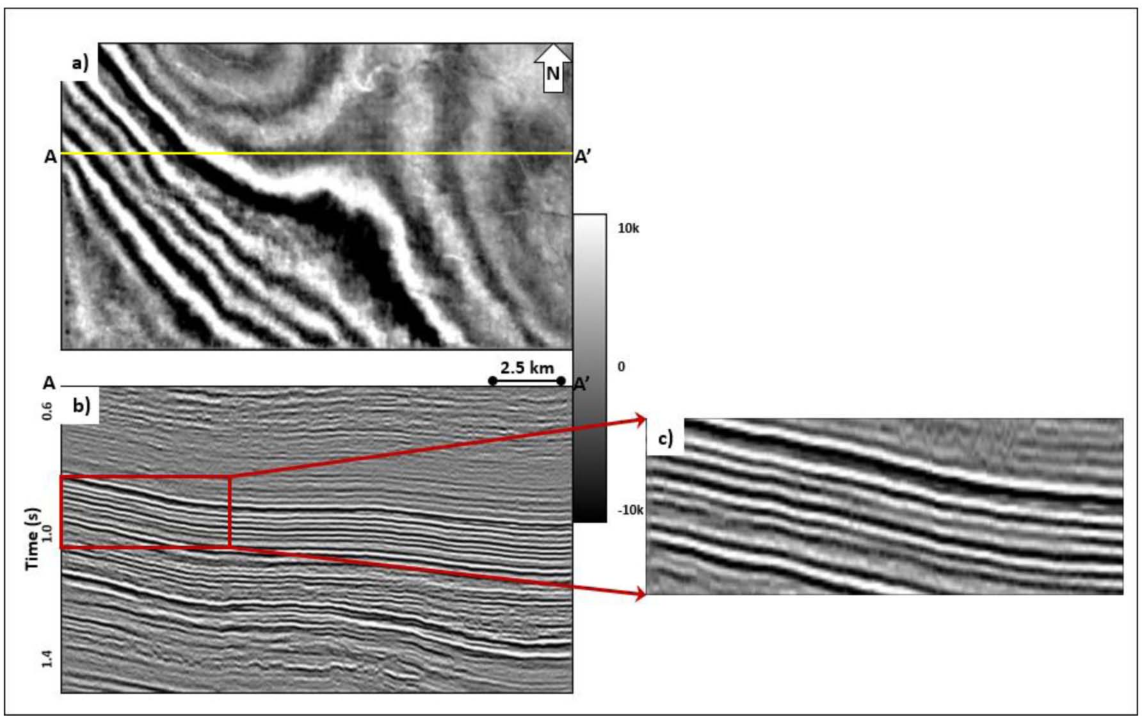

Figure 10—a) Time slice and b) corresponding seismic profile along AA', and c) zooned in section (Figure 10b) of seismic amplitude volume after structure-oriented filtering.

The dip magnitude (Figure 11a) and similarity (Figure 11b) are recalculated after structure-oriented filtering, in which the random noise have been attenuated and acquisition footprint anomalies (red dashed polygon) have been partly suppressed compared to the ones in Figures 7a and 7b. Besides, the structures indicated by black arrows becomes more clears as before.

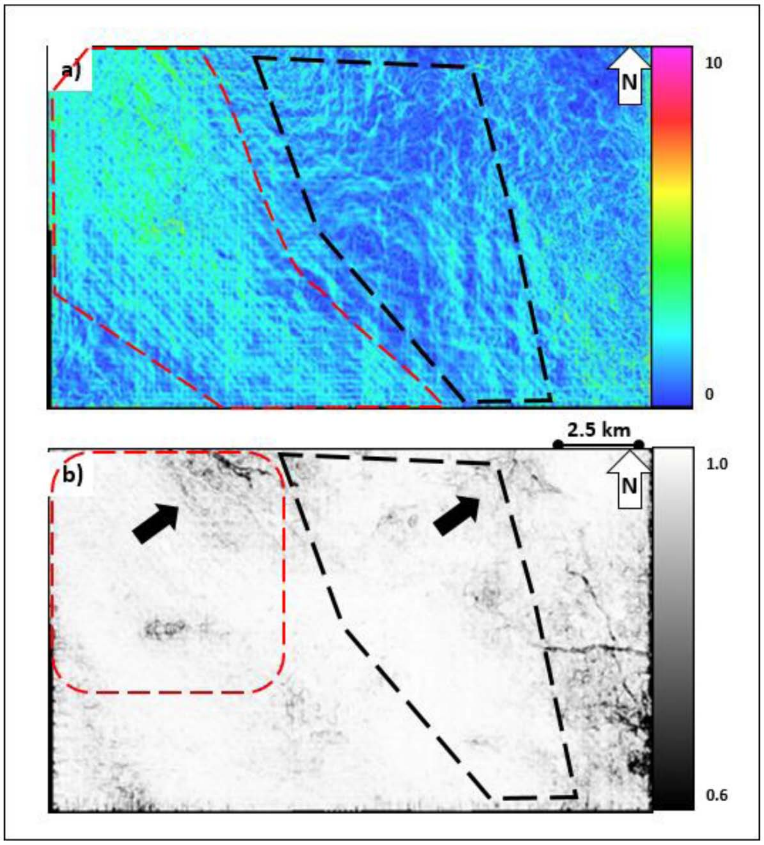

Figure 11—a) Dip magnitude slice and b) coherence slice of the seismic amplitude volume after structure-oriented filtering.

Attribute-Assisted Footprint Suppression

The acquisition footprint artifacts periodically distribute in the large wavenumber zone (short wavelength), while the structural signal focuses in the center zone with small wavenumber position (long wavelength) in 2D wavenumber domain. Figure 12 shows the detailed workflow for this process. Firstly, generate seismic attributes (coherence) which are sensitive to acquisition footprint anomalies. Secondly, apply a vertical median filter to suppress true structural signal and highlight acquisition footprint patch-like artifacts. Thirdly, transform the seismic amplitude volume and filtered seismic attribute volume to 2D waveform domain. Fourthly, apply Laplace-Gaussian (LoG) filter to the filtered seismic attribute of 2D waveform domain, to improve the true structural signal as well as periodic acquisition footprint responses compared to the background energy. Fifthly, a 2D low-pass filter is applied to keep the true structural signal, and a threshold value is set to separate the background energy and the acquisition footprint responses, generating an acquisition footprint mask. Sixthly, the mask can be seen as acquisition footprint position in 2D waveform domain, we apply the mask to the seismic amplitude spectrum to subtract acquisition footprint responses. Seventhly, convert pedestal acquisition footprint responses to 2D spatial domain by reverse 2D waveform transform, and subtract it from original seismic amplitude volume to get ultimate filtered results. In the end, recalculate acquisition footprint sensitive attributes to check the data quality. Recycle the workflow if too much residual acquisition footprint anomalies left.

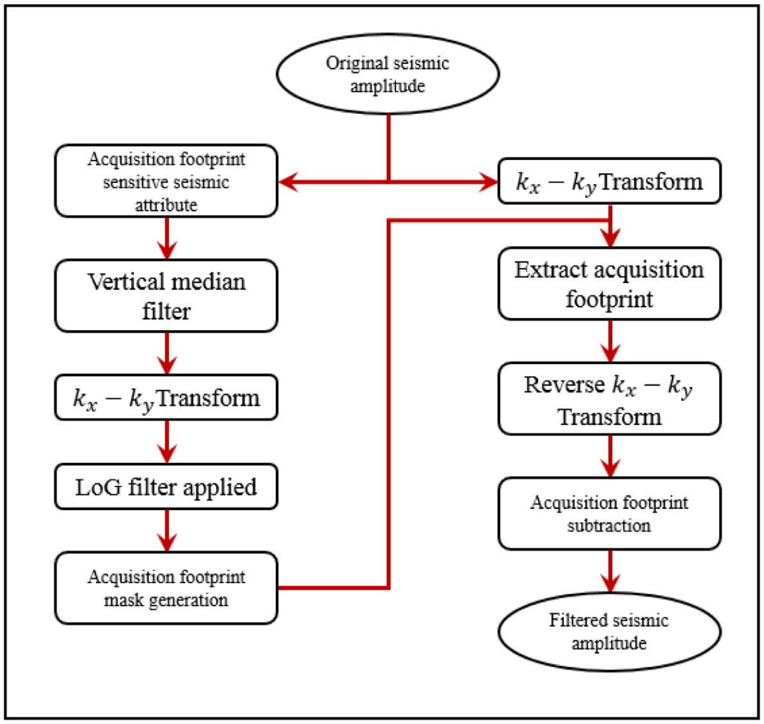

Figure 12—The workflow of attribute-assisted footprint suppression.

We apply attributed-assisted footprint suppression workflow shown above to the seismic amplitude volume (Figure 9) after structure-oriented filtering, to attenuate residual acquisition footprint anomalies. Figure 13 indicates the filtered coherence slice of k_x-k_y domain transformed from the Figure 11b, the application of vertical median filter can effectively enhance acquisition footprint anomalies while rejecting true stratigraphic features. Figure 14a shows the coherence slice of k_x-k_y domain before Laplace-Gaussian (LoG) filtering. The true stratigraphic responses (white arrow) are mainly focused in the small wavenumber zone, and the periodic high energy responses (black and grey arrows) caused by acquisition footprint anomalies are located in the large wavenumber zone. The acquisition footprint responses indicated by black arrow can be easily extracted, while the ones by grey arrows can hardly be recognized due to the minor difference compared to the background energy. The application of Laplace-Gaussian (LoG) filter to the coherence slice of k_x-k_y domain (Figure 14b) can effectively highlight acquisition footprint responses. The acquisition footprint mask (Figure 15a) is generated after 2D low-pass filtering and threshold filtering. Laplace-Gaussian (LoG) filtering in Figure 15b gives us a better acquisition footprint mask, in which the responses indicated by grey arrows are also recognized.

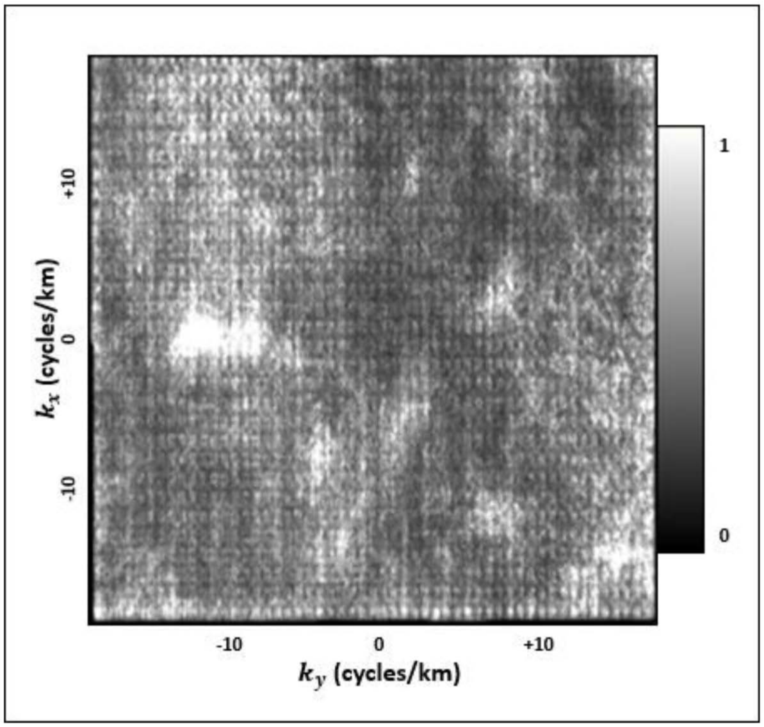

Figure 13—The coherence slice of k_x-k_y domain transformed from the Figure 11b after vertical median filtering.

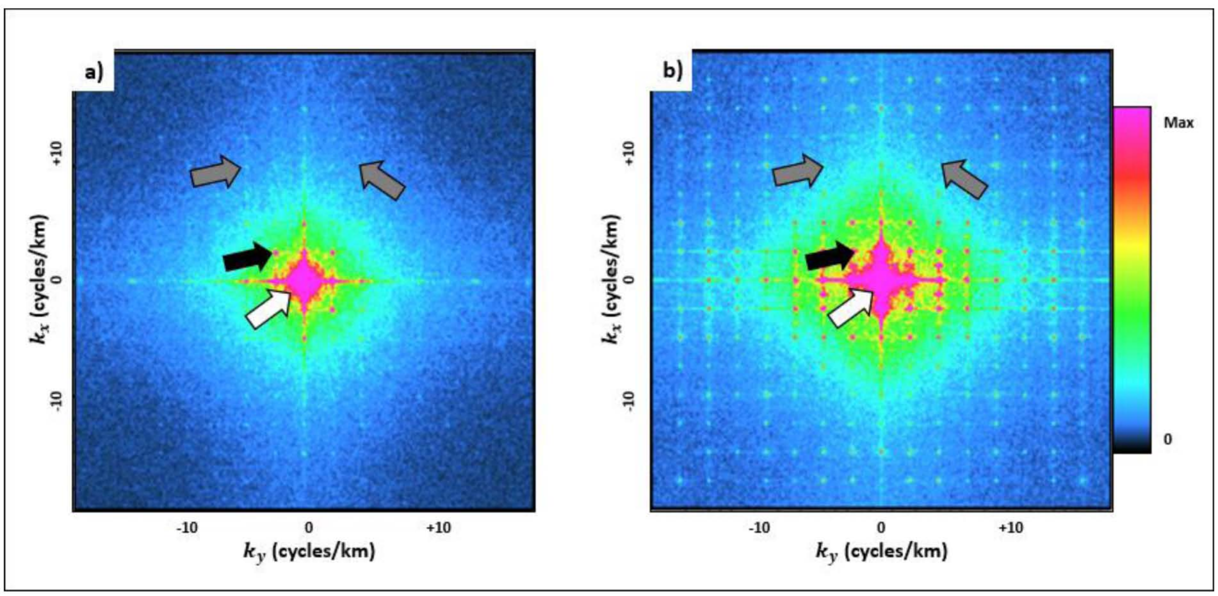

Figure 14—The coherence slice of k_x-k_y domain a) before and b) after Laplace-Gaussian (LoG) filtering.

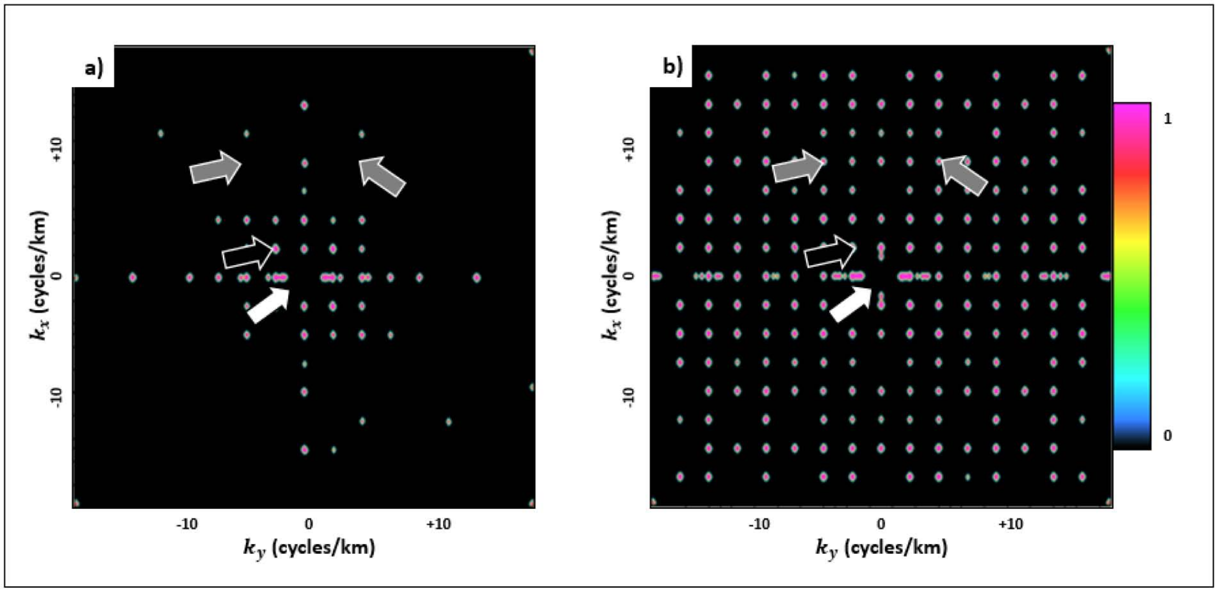

Figure 15—The acquisition footprint mask with 2D low-pass filtering and threshold filtering a) before and b) after Laplace-Gaussian (LoG) filtering.

By extracting acquisition footprint responses of seismic amplitude from 2D waveform transform, and transforming to 2D spatial domain (Figure 16b), we can subtract the coherent noise to get the ultimate results (Figure 16a). Converting seismic amplitude volume after structure-oriented filtering to k_x-k_y domain (Figure 17a), some acquisition footprint processing method had been used due to the existence of the patch-notch (white arrow), while there are still some residual noise left. The 2D waveform transform of the filtered results in Figure 17b indicates that the relevant noise anomalies have been suppressed compared to the one in Figure 8a.

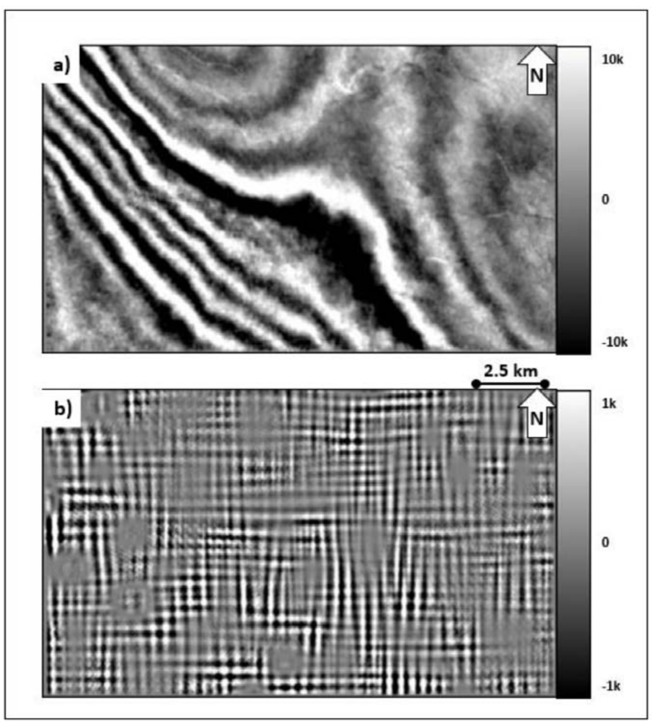

Figure 16—a) Time slice of seismic amplitude volume after acquisition footprint suppression and b) its corresponding extracted modeled noise.

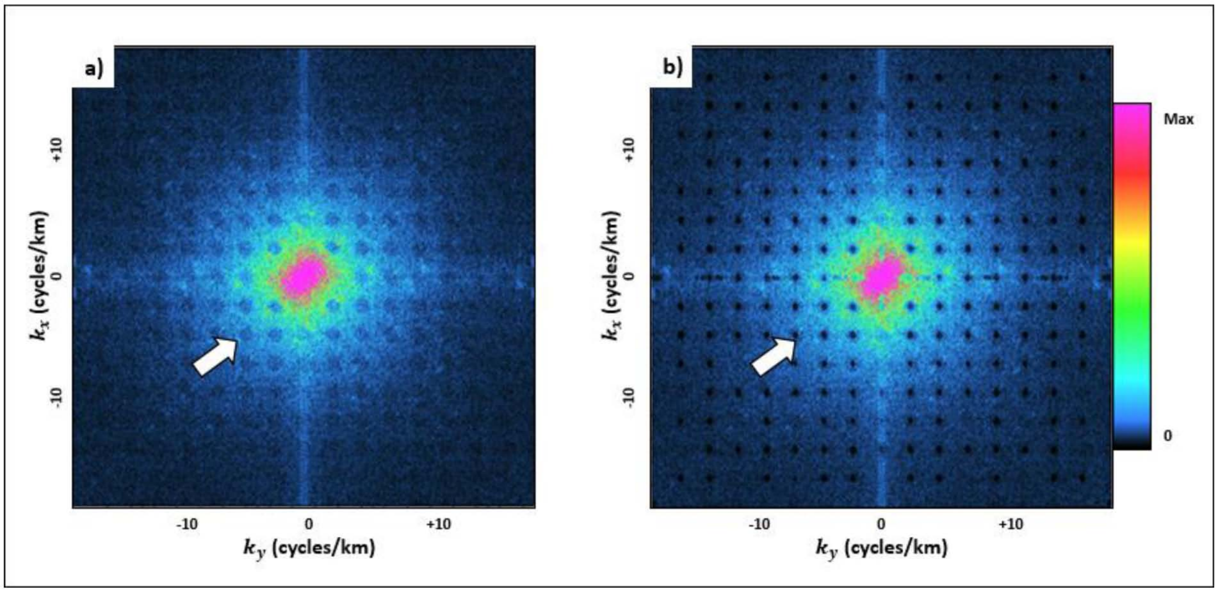

Figure 17—The time slice of amplitude spectrum in kx-ky domain a) before structure-oriented filtering and b) after acquisition footprint suppression.

The acquisition footprint sensitive attributes, dip magnitude (Figure 18a) and coherence (Figure 18b) are recalculated, in which acquisition footprint anomalies are further suppressed. We can hardly recognize the relevant responses in Figures 18a and 18b. And the black indicates the structural signal which used to be blurred in Figure 11b.

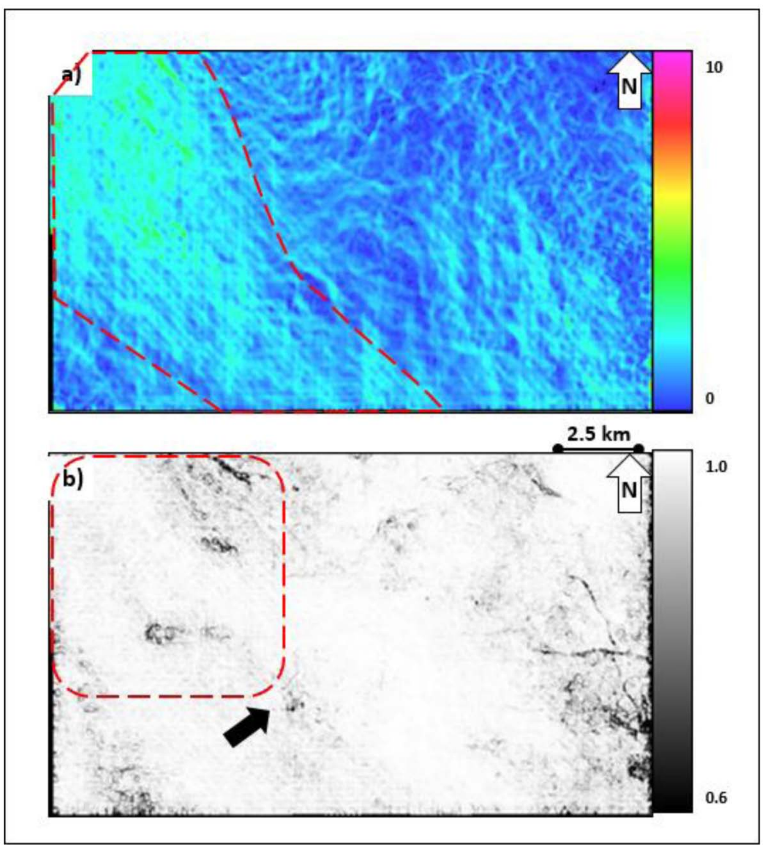

Figure 18—a) Dip magnitude slice and b) coherence slice of the seismic amplitude volume after acquisition footprint suppression.

Conclusions

The random noise and acquisition footprint anomalies due to the acquisition and processing seriously suppresses stratigraphic features, and can easily result in pitfalls during seismic interpretation, seismic attribute analysis as well as seismic inversion.

Attribute-assisted structure-oriented filtering in this paper can effectively remove both non-periodic and partial periodic noise to obtain higher signal to noise ratio (SNR) of post-stack seismic data.

Since the pre-stack seismic date are not usually available for interpreters, attribute-assisted footprint suppression is a powerful tool for the identification and further separation of acquisition footprint anomalies in k_x-k_y domain. Acquisition footprint responses enable seismic attributes to characterize acquisition footprint anomalies that can be used to define notch filters. Therefore, seismic attributes can be used to generate a better acquisition footprint mask. Besides, the Laplace-Gaussian (LoG) filtering can help highlight the seismic responses of both stratigraphic features and acquisition footprint anomalies compared to the background in the k_x-k_y domain.

Acknowledgements

We thank the Research Institute of Petroleum Exploration and Development, CNPC, for the permission to publish the relevant seismic data. We thank the OU Attribute-Assisted Processing and Interpretation Consortium for their support. We especially thank the mentor, Mrs. Xueling Wang, for her kind guidance and devoting help in the past year.

Nomenclature

d_m, d_n	inline and crossline spacing, m
e	Exponential (exp)
j	imaginary number
$\|k\|$	modulus of complex numbers in 2D waveform domain
$\|k\|max$	The maximum modulus of complex numbers in 2D waveform domain
k_x, k_y	The wavenumber in inline and crossline direction
log_σ	Laplace-Gaussian filter in spatial domain
LoG_σ	Laplace-Gaussian filter in 2D waveform domain
m,n	Loop variable
M_{2D},N_{2D}	wavenumber period in inline and crossline direction in 2D waveform transform
M_{Kuw} N_{Kuw}	The half window size in the inline and crossline direction of Kuwahara filter
r_{Kuw}	the radius of Kuwahara filter
s	coherence value in coherence volume
s_{low}, s_{high}	The low and high threshold values which separate the structural features to be preserved from the noise to be smoothed in Kuwahara filter
u	The input signal in 2D spatial domain
u_{attr}	The seismic attribute in 2D spatial domain
u_{mean}	the mean value of Kuwahara filter
u_{orig}	The original value of Kuwahara filter
u_{SOF}	The value after structure-oriented filtering
U	The 2D waveform transform of u
U_{attr}	The 2D waveform transform of u_{attr}
U_{wgt}	The ultimate result in k_x-k_y domain after Laplace-Gaussian filtering and factor weighting
w_{SOF}	The weighted factor in structure-oriented factor
w_k	The wright factor for Laplace-Gaussian filtering

π	PI
σ	Gaussian operator
φ	The phase spectrum of 2D waveform transform
max	The maximum value
NINT	The nearest integer
$+$	addition
$-$	subtraction
$\pm$	addition and subtraction
$\cdot$	multiplication
$/$	division
$\frac{a}{b}$	numerator-denominator
$\lvert\,\rvert$	absolute value
$\sqrt{\ }$	radical sign
$\sum$	accumulation
Δ	The Laplace operator
$\nabla \cdot \nabla$	the divergence of the gradient
( )	parentheses
[ ]	brackets

Reference

Alili, A., Machado, G. and Marfurt, K. J. 2016. Attribute-assisted footprint suppression using a 2D continuous wavelet transform. 86th Annual International Meeting, SEG, Expanded Abstracts: 1898-1902.

Bahorich, M., Motsch, A., Lauthlin, K. and Partyka, G. 2002. Amplitude responses image reservoir. *Hart's E&P, January*: 59-61.

Barnes, A. E. 2005. Fractal analysis of fault attributes derived from seismic discontinuity data. 67th Annual Conference and Exhibition, EAGE, Extended Abstracts: P318.

Buttkus, B. 2000. Spectral analysis and filter theory in applied geophysics. Springer.

Cahoj, M. P., Verma, S., Hutchinson, B. and Marfurt, K. J. 2016. Pitfalls in processing: An application of seismic modeling to investigate acquisition footprint. *Interpretation*: **4**(2): SG1-SG9.

Davogustto, O. and Marfurt, K. J. 2011. Footprint suppression applied to legacy seismic data volumes to appear in the GCSSEPM 31st Annual Bob. F. Perkins Research Conference.

Drummond, J. M., Budd, J. L. and Ryan, J. W. 2000. Adapting to noisy 3D data-attenuating the acquisition footprint. 70th Annual International Meeting, SEG, Expanded Abstracts: 9–12.

Falconer, S. and Marfurt, K. J. 2006. Attribute-driven footprint suppression. 76th Annual Conference and Exhibition, SEG Expanded Abstracts: 2667-2671.

Finn, C. J. 1986. Estimation of three dimensional dip and curvature from reflection seismic data. M.S. thesis, University of Texas, Austin.

Gulunay, N., Sudhaker, V., Gerrard, C. and Monk, D. 1993. Prediction filtering for 3D post-stack data. 63rd Annual International Meeting, SEG, Expanded Abstracts: 1183-1186.

Gulunay, N. 2000. 3D acquisition footprint removal. 62nd Annual International Conference and Exhibition, EAGE, Extended Abstracts: L0017.

Hill, S., Shultz, M. and Brewer, J. 1999. Acquisition footprint and fold of stack plots. *The Leading Edge* **18**: 686-695.

Kuwahara, M., Hachimura, K., Eiho, S. and Kinoshita, M. 1976. Digital processing of biomedical images. Plenum Press, 187-203.

Lin, T., Marfurt, K. J. and Zhang, B. 2016. Attribute-assisted footprint suppression with LoG filter. 86th Annual International Meeting, SEG, Expanded Abstracts: 4705-4709.

Lin, T., Zhang, B., Guo S. and Marfurt, K. J. et al. 2013. Spectral decomposition of time-versus depth-migrated data.

Lin, T., Zhang, B., Liu, X. and Marfurt, K. J. 2018. Structure Constrained Spectral Decomposition Based on Matching-Pursuit Method. 88th Annual International Meeting, SEG, Expanded Abstracts: 1778-1782.

Liu, J. and Marfurt, K. J. 2005. Matching Pursuit Decomposition Using Morlet Wavelets. 75th Annual International Meeting, SEG, Expanded Abstracts: 786-790.

Liu, J. and Marfurt, K. J. 2007. Instantaneous spectral attributes to detect channels. *Geophysics* **72**: P23-P31.

Luo, Y., al-Dossary, S. and Marhoon, M. 2002. Edge-preserving smoothing and applications. *The Leading Edge* **21**: 136–158.

Marfurt, K. J. 2006. Robust estimates of dip and azimuth. *Geophysics* **71**: P29-P40.

Marfurt. K. J. and Alves, T. M. 2014. Pitfalls and limitations in seismic attribute interpretation of tectonic features. *Interpretation* **3**(1): SB5-SB15.

Marfurt, K. J., Kirlinm R. L., Farmer, S. H. and Bahorich, M. S. 1998a. 3-D seismic attributes using a running window semblance-based algorithm. *Geophysics* **63**: 1150-1165.

Marfurt, K. J., Scheet, R. M., Sharp, J. A. and Harper, M. G. 1998b. Suppression of the acquisition footprint for seismic sequence attribute mapping. *Geophysics* **63**: 1024-1035.

Marr, D. and Hildreth, E. 1980. Theory of edge detection. Proceedings of the royal Society of London, Series B, *Biological Science* **207**: 187-217.

Partyka, G., Gridley, J. and Lopez, J. A. 1999. Interpretational applications of spectral decomposition in reservoir characterization. *The Leading Edge* **18**: 353-360.

Qin, F., Burnstad, R. M. and Leger, P. C. 2012. An effective *f-k* domain random noise suppression technique applied to a land data set. 82nd Annual International Meeting, SEG, Expanded Abstracts: 4609-4612.

Xu, S., Zhang, Y. and Lambare, G. 2005. Antileakage Fourier transform for seismic data regularization in higher dimensions. *Geophysics* **70**(6): V87–V95.

Wang, Y. 2007. Seismic time-frequency spectral decomposition by matching pursuit. *Geophysics* **72**(1): v13–v20.

Wang, Y. 2010. Multichannel matching pursuit for seismic trace decomposition. *Geophysics* **75**(4): v61-v66.